Received: 18 April 2024 | Revised: 4 July 2024 | Accepted: 11 July 2024

DOI: 10.1002/pro.5123

RESEARCH ARTICLE

THE PROTEIN SOCIETY WILEY

Cellular turnover and degradation of the most common missense cystathionine beta-synthase variants causing homocystinuria

Ela Mijatovic | **Kelly Ascenção** | **Csaba Szabo** | **Tomas Majtan**

Section of Pharmacology, Faculty of Science and Medicine, University of Fribourg, Fribourg, Switzerland

Correspondence
Tomas Majtan, Department of Pharmacology, University of Fribourg, Faculty of Science and Medicine, Chemin du Musee 18, PER17, Fribourg, 1700, Switzerland.
Email: tomas.majtan@unifr.ch

Funding information
University of Fribourg, Grant/Award Number: 22-15; Swiss National Science Foundation, Grant/Award Number: 10.001.133

Review Editor: Aitziber L. Cortajarena

Abstract

Homocystinuria (HCU) due to cystathionine beta-synthase (CBS) deficiency is the most common inborn error of sulfur amino acid metabolism. Recent work suggests that missense pathogenic mutations—regardless of their topology—cause instability of the C-terminal regulatory domain, which likely translates into CBS misfolding, impaired assembly, and loss of function. However, it is unknown how instability of the regulatory domain translates into cellular CBS turnover and which degradation pathways are involved in CBS proteostasis. Here, we developed a human HEK293-based cellular model lacking intrinsic CBS and stably overexpressing wild-type (WT) CBS or its 10 most common missense HCU mutants. We found that HCU mutants, except the I278T variant, expressed similarly or better than CBS WT, with some of them showing impaired oligomerization, activity and response to allosteric activator S-adenosylmethionine. Cellular stability of all HCU mutants, except P49L and A114V, was significantly lower than the stability of CBS WT, suggesting their increased degradation. Ubiquitination analysis of CBS WT and two representative CBS mutants (T191M and I278T) showed that proteasomal degradation is the major pathway for CBS disposal, with a minor involvement of lysosomal-autophagic and endoplasmic reticulum-associated degradation (ERAD) pathways for HCU mutants. Proteasomal inhibition significantly increased the half-life and activity of T191M and I278T CBS mutants. Lysosomal and ERAD inhibition had only a minor impact on CBS turnover, but ERAD inhibition rescued the activity of T191M and I278T CBS mutants similarly as proteasomal inhibition. In conclusion, the present study provides new insights into proteostasis of CBS in HCU.

KEYWORDS
conformational disorder, folding, proteostasis, ubiquitin signaling

1 | INTRODUCTION

Human cystathionine-beta synthase (CBS) polypeptide has a unique multi-domain architecture consisting of the N-terminal heme-binding domain, a central catalytic core housing the pyridoxal-5′-phosphate (PLP) cofactor, and the C-terminal S-adenosylmethionine (SAM)-binding regulatory domain (Zuhra et al., 2020). CBS is a pivotal enzyme in sulfur amino acid metabolism that governs the flow of organic sulfur by regulating the flux of homocysteine between remethylation and transsulfuration pathways. CBS irreversibly diverts homocysteine from the methionine cycle to cysteine synthesis by catalyzing its condensation with serine. Substrate promiscuity allows CBS for alternative reactivity metabolizing cysteine alone or with homocysteine, generating hydrogen sulfide (H_2S) (Majtan et al., 2018; Singh et al., 2009), thus making CBS one of a few enzymatic sources of this gasotransmitter with multiple roles in mammalian pathophysiology (Cirino et al., 2023). Upregulation of CBS in cancer (Sen et al., 2016; Szabo et al., 2013) or overexpression of CBS in Down Syndrome (Panagaki et al., 2019, 2022) result in H_2S overproduction, which regulates cellular bioenergetics, cell proliferation, and cell viability in the above conditions. On other hand, deficiency of CBS—primarily due to inactivating missense mutations in the CBS gene—leads to the accumulation of homocysteine, a biochemical hallmark of classical homocystinuria (HCU) (Morris et al., 2017). HCU is an inborn error of metabolism clinically manifesting by connective tissue defects, cognitive impairment and increased risk of thromboembolism and stroke (Mudd et al., 1985).

Our previous studies on recombinantly expressed and purified pathogenic CBS variants suggested that the majority of the pathogenic missense mutations do not target key catalytic residues or do not impair binding of cofactors (heme, PLP, and SAM), but affect the conformation, oligomerization, and overall stability of this enzyme (Hnizda et al., 2012; Majtan et al., 2010; Pey et al., 2013). Very low stability of some CBS variants—including the most prevalent in population CBS I278T—essentially precluded its purification and characterization when overexpressed in *Escherichia coli*. Interestingly, calorimetric characterization of seven pathogenic CBS variants suggested that the presence of missense mutations anywhere within CBS polypeptide result in an impaired kinetic stability of the C-terminal regulatory domain, that is, a faster rate of unfolding destabilizing entire protein compared to the wild-type CBS (WT) (Pey et al., 2013). In addition to being responsible for binding SAM and regulating CBS activity, this domain plays a central role in quaternary assembly and oligomerization of CBS (McCorvie et al., 2024; Pey et al., 2016). Furthermore, cultured skin fibroblasts from HCU patients showed the absence of native CBS tetramers: CBS was predominantly sequestered into high molecular weight aggregates devoid of heme (Janosik et al., 2001). These observations, when taken together, suggest that HCU should be viewed as a protein conformational disorder with protein misfolding and instability as the main mechanism resulting in CBS deficiency.

The protein homeostasis (proteostasis) network as a quality-control machinery integrates cellular factors responsible for protein synthesis, folding, and conformational maintenance of the newly synthesized proteins as well as their controlled degradation (Jayaraj et al., 2020). While molecular chaperones—including a wide array of heat shock proteins—assist protein folding and adoption of native conformation (Balchin et al., 2020), the main orchestrators of the recycling of proteins that are no longer needed or removal of dysfunctional and misfolded proteins are the ubiquitin–proteasome system (UPS) and the autophagy–lysosomal pathway (ALP). Both degradation systems depend on ubiquitination, a process in which one or more ubiquitin polypeptides are covalently attached onto lysine residues of target proteins (Suresh et al., 2016). Ubiquitination is a highly regulated process catalyzed by a sequential action of three different classes of enzymes: ubiquitin-activating (E1), ubiquitin-conjugating (E2), and ubiquitin-ligating enzymes (E3). UPS and ALP crosstalk through endoplasmic reticulum-associated degradation (ERAD), which prevents the accumulation of misfolded proteins within the ER (Araki & Nagata, 2011). Our recent study showed that the expression of pathogenic CBS variants results in a dysregulation of small heat shock proteins, induces ER stress and reduces the steady-state levels and the activity of the studied CBS variants. Importantly, genetic or pharmacological manipulations of HSP70 improves the folding of the CBS variants and partially rescues their activity (Collard & Majtan, 2023). More impressive CBS functional rescue has been achieved by use of proteasome inhibitors in several transgenic models of HCU expressing different pathogenic missense CBS variants including I278T or R266K (Gupta et al., 2013, 2017). These data suggest that UPS is the main degradation pathway for CBS, but the potential involvement of other systems has not been evaluated. Importantly, even though proteasome inhibitors rescued CBS steady-state levels in the liver of transgenic HCU mice, the functional correction was often more variable in terms of the recovery of CBS activity or plasma homocysteine levels (Gupta et al., 2023). In addition to proteotoxic stress resulting from CBS misfolding, subsequent buildup of homocysteine could contribute to dysregulated CBS proteostasis. Elevated concentrations of homocysteine are known to

diminish autophagy, to induce mitochondrial dysfunction, to aggravate ER stress and lead to apoptosis of neuronal cells; these effects were all ameliorated by chemical chaperone 4-phenylbutyric acid (Kaur et al., 2023).

In this study, we employed a new cell-based model of HCU in order to gain more insight into the relationship between CBS folding and the various degradation pathways involved in proteostasis of CBS. Furthermore, we have determined whether pharmacological inhibition of the various degradation pathways may beneficially affect CBS stability of activity.

2 | MATERIALS AND METHODS

2.1 | Cell culture

Unless specified otherwise, a subclone of the human embryonic kidney 293 cell line HEK293A (Invitrogen) showing more adherent and flat morphology compared to the parent line was used for all the experiments described in this report. The cells were maintained by culturing in Dulbecco's Modified Eagle Medium (DMEM; Gibco) supplemented with 10% fetal bovine serum (FBS; Invitrogen) and 1% penicillin–streptomycin (Gibco) in a humidified incubator with 5% CO_2 atmosphere at 37°C.

The HEK293 cells lacking CBS (CBS KO) were generated by CRISPR-Cas9 approach. Specifically, the gRNA targeting CBS gene (GACGGAGCAGACAACCTACG) was designed by using the Sanjana lab design guide tool (http://guides.sanjanalab.org/), synthesized by Microsynth and introduced into lentiCRISPR v2 plasmid (cat# 52961; Addgene). The plasmid was transformed into *E. coli* Stable (NEB) and a random ampicillin-resistant colony was further propagated in LB medium supplemented with 100 μg/mL ampicillin. After purification using PureLink HiPure midiprep kit (Invitrogen), the integrity of the plasmid was verified by digestion with *Bgl*II and *Nde*I restriction endonucleases (NEB) and confirmed by DNA sequencing (Microsynth). The lentiviral particles for HEK293 transduction were produced and used as previously described (Ascencao et al., 2021). Briefly, viral particles were produced in HEK293T cells (ATCC) using the third-generation lentiviral system. Medium containing lentiviral particles was collected 24 h after transfection, filtered via a 0.45 μm filtration unit, aliquoted and stored at −80°C. The HEK293A cells were transduced with lentiviral particles in the presence of 6 μg/mL protamine sulfate. Puromycin (1 μg/mL) was added to the culture 72 h after transduction to select for CBS KO cells. Single cell clones were subsequently generated by plating the cells at low density into a 96-well plate. Ten single cell clones were then randomly picked, propagated, and confirmed for the lack of CBS protein by Western blot analysis.

Stable cell lines expressing CBS WT as control or pathogenic HCU variants were prepared by lentiviral transduction of HEK293 CBS KO cells. Specifically, codon optimized human CBS WT carrying myc-tag and 6×His-tag at its N- and C-termini, respectively, was synthesized by Genscript and subcloned using pLentiCMV-Blast-empty (w263-1) plasmid (cat# 17486, Addgene) directionally into unique *Sal*I and *Xba*I restriction endonuclease sites. Pathogenic missense HCU mutation P49L, A114V, R125Q, T191M, R266K, I278T, G307S, R366C, D444N, or S466L were introduced by site directed mutagenesis by Genscript using CBS WT plasmid as a template. All constructs were verified by DNA sequencing (Genscript). Supplied plasmids were used for the generation of lentiviral particles as described above. The HEK293A CBS KO cells were then transduced with the obtained lentiviral particles in the presence of 6 μg/mL protamine sulfate. Blasticidin S (45 μg/mL) was added to the culture 72 h after transduction to select for cells carrying CBS construct.

For ubiquitination studies, HEK293A CBS KO cells overexpressing CBS WT or the selected HCU mutants (T191M or I278T) were cultured in a six-well plate until reaching 70%–80% confluency. Subsequently, the cells were transiently transfected using JetOptimus reagent (Polyplus) according to the manufacturer's recommendation with plasmid for constitutive co-expression of hemagglutinin (HA)-tagged ubiquitin WT, KO, K6, K11, K29, K48, or K63 variants (cat# 17608, 17603, 22900, 22901, 22903, 17605, and 17606, respectively; Addgene) (Lim et al., 2005; Livingston et al., 2009). After overnight incubation, the cells were placed on ice, washed with cold phosphate-buffered saline (1× PBS) twice, lysed using ice-cold modified RIPA buffer (25 mM Tris–HCl pH 7.6, 150 mM NaCl, 1% Triton X-100, and 0.1% sodium dodecyl sulfate (SDS)) supplemented with Halt protease and phosphatase inhibitor cocktail and Pierce universal nuclease for cell lysis (both from ThermoScientific). Cell lysates were transferred into Eppendorf tubes, briefly sonicated using bath sonicator and clarified by centrifugation at 21,000 × g for 20 min at 4°C. Protein concentration of the lysates was determined by the BCA kit (ThermoScientific).

2.2 | Cell proliferation assay

The proliferation of new cell lines was characterized using two different assays. Amount of genomic DNA in cells seeded at ~80% confluency was quantified after 24 h incubation in 5% CO_2 atmosphere at 37°C by using the

colorimetric Cell proliferation BrdU ELISA kit (EMD Millipore) according to manufacturer's protocol. Data from three biological and three technical replicates were pooled together, normalized to a control (HEK293 A CBS KO cells stably expressing CBS WT variant) and expressed as percentage ± SEM.

To determine doubling time of the newly generated HCU cell models and respective WT controls, we monitored the growth of the cells over a 120 h period using Cytation 5 imager equipped with robotic arm and BioSpa8 humidified CO_2 plate incubator (Agilent). Cells seeded into a 96-well plate (7000 cells/well) were allowed to fully attach overnight and then transferred into BioSpa8 incubator. Cell proliferation was recorded every 6 h using 10× magnification objective in two different areas within each well in two channels: brightfield for visualization and high-contrast brightfield with −200 μm focal offset compared to brightfield for automated cell counting. Image pre-processing and cellular analysis were done using Gen5 software (Agilent). Data from two different well areas of three biological and three technical replicates were pooled together and cell confluency ± SEM was calculated.

2.3 | Cell viability assay

The viability of new cell lines was determined using MTT assay as described previously (Ascencao et al., 2021; Casili et al., 2022). Briefly, cells were seeded at 80% confluency into a 96-well plate and following day incubated with 0.5 mg/mL MTT for 1 h. To visualize the mitochondria-dependent enzymatic conversion of the water-soluble yellow MTT into an insoluble purple formazan, the culture medium was removed and 100 μL of DMSO was added to each well followed by shaking of the plate to solubilized formazan. Absorbance at 590 nm was measured using a SpectraMax iD3 plate reader (Molecular Devices). Data from three biological and three technical replicates were pooled together, normalized to a control (HEK293 A CBS KO cells stably expressing CBS WT variant) and expressed as percentage ± SEM.

2.4 | Protein electrophoresis and Western blot analysis

Cell lysates to be analyzed by Western blotting were either mixed with 2× Novex Tris-glycine Native sample buffer (Invitrogen) for native electrophoresis or with 4× Bolt LDS sample buffer containing sample reducing agent (Invitrogen) for reducing denatured electrophoresis. Denaturation was performed at 95°C for 10 min. Native proteins were resolved in NativePAGE 4%–16% Bis–Tris gels in 1× NativePAGE running buffer at 4°C, while reduced, denatured proteins were separated in NuPAGE 4%–12% Bis–Tris gels in 1× NuPAGE MES SDS running buffer (all from Invitrogen). Subsequently, proteins were transferred onto the PVDF membrane using an iBlot 2 gel transfer device (Invitrogen). Membranes were blocked in 5% non-fat milk in 1×TBTS (Tris buffered saline supplemented with 0.1% Tween 20) for 1 h at room temperature (RT), followed by incubation with the primary antibody while gently agitating either for 1 h at RT or overnight at 4°C. Primary antibodies were diluted in 5% BSA–TBST or 5% milk–TBST solution as follows: anti-CBS (1:2000; Abnova cat#H00000875-M01), anti-beta-actin (1:5000; Sigma cat#A1978), anti-ubiquitin (1:1000; CST cat#3936), or anti-HA-tag (1:1000; CST cat#3724). After washing with TBST for 5 min three times, blots were incubated with anti-rabbit or anti-mouse IgG HRP-conjugated antibody (1:5000; CST cat#7074 or 7076) in 5% milk-TBST for 1 h at RT. After washing with TBST for 5 min twice and TBS for 5 min twice, the proteins were visualized with Radiance Plus chemiluminescence substrate using the Imaging System 300 (both from Azure Biosystems). Captured images were analyzed using the ImageJ software (NIH, Bethesda, MD, USA).

2.5 | Determination of CBS half-life

Cellular turnover of CBS was evaluated by employing a novel non-radioactive method based on incorporation of L-azidohomoalanine (AHA), a biorthogonal analog of methionine, as described previously (Morey et al., 2016, 2021). The HEK293A CBS KO cells stably expressing WT or mutant CBS were grown to ∼80% confluency in a six-well plate. The cells were then washed with methionine-deficient DMEM (Gibco) containing 10% dialyzed FBS (Gibco), 2 mM GlutaMax (Gibco), 1 mM pyruvate (Cytiva) and 200 μM cystine hydrochloride (Sigma) followed by live-labeling for 4 h (pulse) in a methionine-deficient DMEM supplemented with 75 μM AHA (Sigma). The AHA pulse was terminated by removing the labeling medium and washing with a complete standard medium, then incubated in the same medium for up to 24 h at 37°C. Immediately after the pulse (0 h) and at designated timepoints during the chase period (2, 6, 9, and 24 h), the cell lysates were prepared as described above except the modified RIPA buffer was additionally supplemented with freshly prepared 10 mM N-ethylmaleimide (NEM; Sigma) and 10 mM iodoacetamide (IAA; Sigma).

To assess the impact of inhibition of UPS, ALP, or ERAD on CBS turnover, the cells were treated with

20 nM bortezomib (BRB; Sigma) (Chen et al., 2021; Gelman et al., 2013), 100 nM bafilomycin (BAF; Sigma) (Park et al., 2017; Purnell & Fox, 2013; Yamamoto et al., 1998) and 10 μM eeyarestatin I (ESI; Sigma) (McKibbin et al., 2012; Park et al., 2017), respectively, during both the pulse and the chase periods.

To determine the half-life of CBS, cell lysates (100 μg) diluted to 0.2 mg/mL in a modified RIPA were incubated with a house-made rabbit polyclonal anti-CBS antibody (1:250) (Kraus & Rosenberg, 1983) on a rocking platform at 4°C overnight followed by pulldown of the CBS–IgG complexes by 25 μL of washed Pierce protein A/G magnetic beads (ThermoScientific) on a rocking platform at RT for 1 h. Immunoprecipitated (IPed) CBS was washed 4× using TBST and subsequently reacted with 10 μM IRDye800-DBCO (LI-COR) in 1× PBS for 1 h at RT to allow click-chemistry conjugation of AHA with the fluorescent dye. After removal of unreacted dye, labeled CBS was released from the beads and denatured in 2× LDS sample buffer supplemented with 1× reducing agent (both from Invitrogen) at 95°C for 10 min. Equal volumes of eluted CBS IPs were separated on SDS–PAGE as described above. However, before Western blot analysis to assess total amounts of CBS in the IPs, the amounts of AHA-labeled CBS were visualized and quantified by fluorescent in-gel detection using Odyssey DLx imaging system (LI-COR).

For the calculation of the half-life of CBS, we assumed that the amount of fluorescent AHA/IRDye800-labeled CBS decays exponentially following first-order kinetics. Therefore, fluorescent intensities of AHA/IRDye800-labeled CBS corrected by the levels of total IPed CBS were plotted over time and rate constants as well as half-lives were determined using one-phase decay function in Prism software (GraphPad).

2.6 | Anti-HA immunoprecipitation

For ubiquitination studies, proteins including CBS modified with HA-tagged ubiquitin variants as described above were captured on 25 μL of monoclonal anti-HA magnetic beads (Sigma) from 100 μg of total protein diluted to 0.2 mg/mL in a modified RIPA buffer at 4°C overnight. The IP samples were washed and eluted essentially as described above for CBS IPs.

2.7 | CBS activity assay

CBS activity was assessed in both cell lysates and live cells. In-gel CBS activity staining was performed as described previously (Willhardt & Wiederanders, 1975). Briefly, cell lysates (10 μg/lane) were resolved in 4%–12% native PAGE as described above. The gel was then washed twice in water and then submerged into the staining solution (100 mM Tris–HCl pH 8.0, 20 mM cysteine, 50 mM beta-mercaptoethanol, 100 μM PLP, and 200 μM lead acetate) both in the absence and presence of 200 μM SAM. The gels were gently shaking at 37°C until the active CBS bands became apparent. The reaction was terminated after the same amount of time for both conditions by replacing the staining solution for 7% acetic acid, the gels were scanned and the CBS activity quantified by densitometry using ImageJ.

CBS activity in the lysates was also determined employing the H_2S-specific fluorescent probe 7-azido-4-methylcoumarin (AzMC; Sigma) as described previously (Thorson et al., 2013). The reaction (200 μL total volume) containing 50 mM Tris–HCl pH 8.6, 5 μM PLP, 10 μM AzMC, 10 μg of cell lysate was initiated after 10 min equilibration at 37°C with a mixture of substrates yielding final concentrations of 2 mM cysteine and 500 μM homocysteine. The assay in the absence or presence of 200 μM SAM was followed for 90 min at 37°C measuring fluorescent intensities in 5 min intervals (excitation 365 nm, emission 450 nm). To account for a possible interference from other H_2S-producing enzyme, most notably the second enzyme of transsulfuration pathway cystathionine gamma-lyase (CGL), selected samples were assayed in the absence or presence of 3 mM propargylglycine (PAG), a specific inhibitor of CGL (Asimakopoulou et al., 2013). All measurements were performed in triplicates using Spectramax M5 microplate reader (Molecular Devices) and analyzed by Prism software.

Lastly, CBS activity was also determined in live cells as described previously (Petrosino et al., 2022). Specifically, HEK293A CBS KO cells stably expressing WT or mutant CBS (T191M and I278T) were seeded into a six-well plate (500,000 cells/well targeting 50% confluency after overnight incubation). Next morning, 20 nM BRB, 100 nM BAF, 10 μM ESI or vehicle for the untreated controls was added in the media to the cells. After 24 h incubation, the medium was replaced by freshly prepared, sterile-filtered 100 μM AzMC in Hank's balanced salt solution (HBSS; Gibco) and the cells were incubated for additional 1 h at 37°C. Brightfield and fluorescent AzMC signal were captured and analyzed using the Cytation 5 multimodal reader operated by Gen5 software (both from Agilent). Single image area was 694 × 694 μm and at least two areas per biological and technical replicate (i.e., different well) were captured using 20× objective and analyzed.

2.8 | Statistical analysis

Unless otherwise noted, all experiments were performed in three independent replicates and the experimental data are presented as means with standard errors of the mean (SEMs). Statistical significance was determined by using one-way ANOVA with Dunnett's test or two-way ANOVA with Tukey's post hoc test in Graphpad Prism software. Cellular turnover of CBS WT and HCU variants was statistically evaluated by extra sum of squares F test. Differences with the p value less than 0.05 were considered significant and marked by asterisk (*) or hashtag (#).

3 | RESULTS

3.1 | Establishment and validation of a novel cell-based model of HCU

To gain better understanding about proteostasis of mutant CBS, we generated a novel cellular model of HCU using human HEK293 cells of kidney origin. Native expression of CBS was abolished by CRISPR-Cas9 and stable cell lines expressing CBS WT as control or pathogenic HCU variants were prepared by lentiviral transduction of HEK293 CBS KO cells as described in Section 2. We modeled 10 of the most common missense pathogenic CBS alleles covering the entire sequence of the protein, namely P49L, A114V, R125Q, T191M, R266K, I278T, G307S, R336C, D444N, and S466L (Figures 1 and 2). Stable expression of pathogenic CBS variants in HEK293A cells lacking intrinsic CBS did not have any significant impact on cell proliferation and doubling time (Figure 1a), cell proliferation as determined by the BrdU assay (Figure 1b), and cell viability as determined by the MTT assay (Figure 1c) compared to a control cell line expressing CBS WT variant. In the next step, we prepared cell lysates and quantified CBS activity using AzMC fluorometric assay (Figure 1d). We observed ~3-fold increases of the enzymatic activity in response to 200 μM SAM with the CBS WT, P49L, A114V, R266K and a lesser degree of activation with the R125Q and

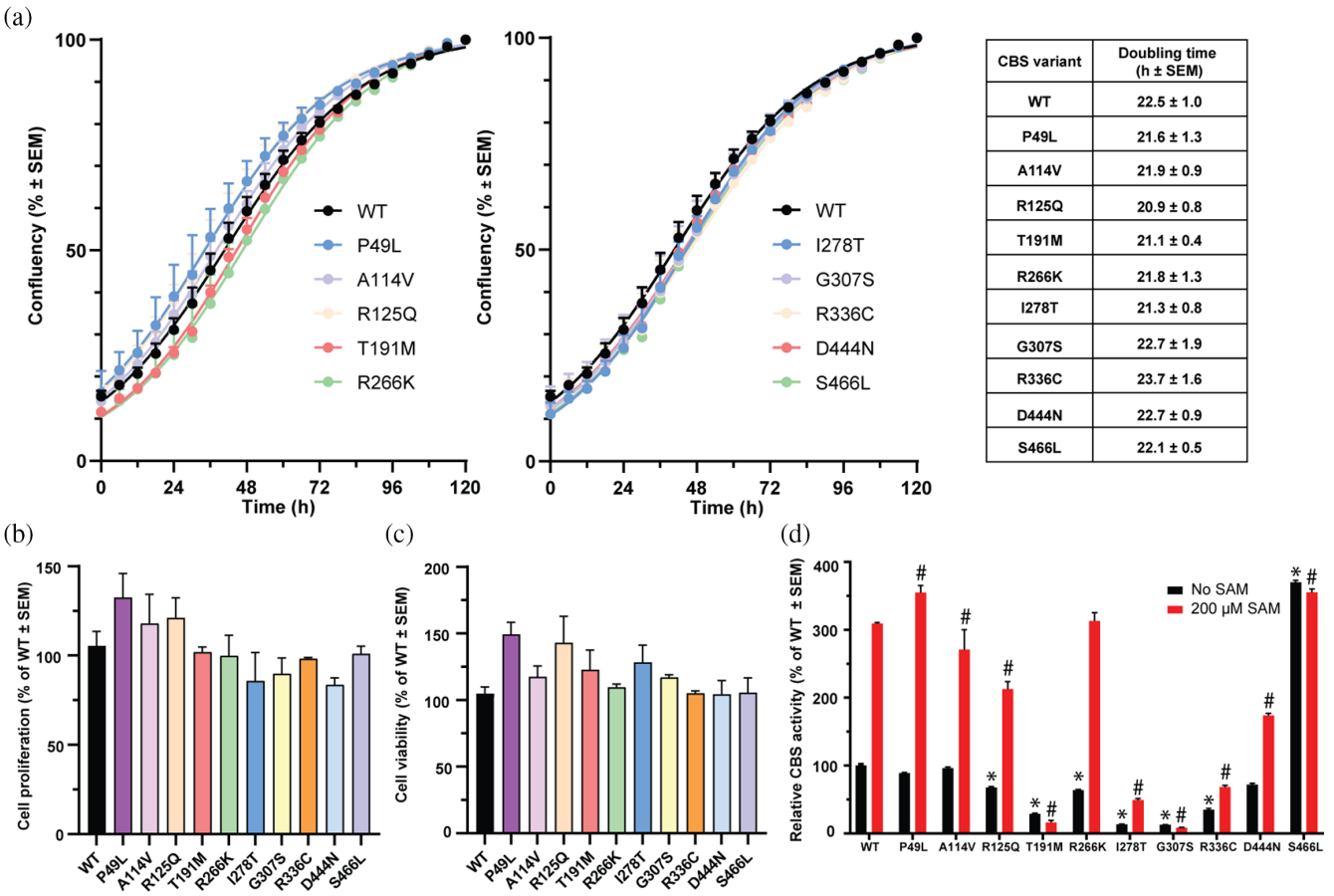

CBS variant	Doubling time (h ± SEM)
WT	22.5 ± 1.0
P49L	21.6 ± 1.3
A114V	21.9 ± 0.9
R125Q	20.9 ± 0.8
T191M	21.1 ± 0.4
R266K	21.8 ± 1.3
I278T	21.3 ± 0.8
G307S	22.7 ± 1.9
R336C	23.7 ± 1.6
D444N	22.7 ± 0.9
S466L	22.1 ± 0.5

FIGURE 1 New cellular model of HCU. (a) Growth curves of HEK293A CBS KO cells stably expressing the designated CBS variant. Doubling times determined from the growth curves are summarized in the table on the right. (b) Cell proliferation rate as determined by the BrdU assay. (c) Cell viability assay as determined by the MTT assay. (d) CBS activity assay (10 μg/assay) of clarified cell lysates in the absence and presence of 200 μM SAM. Significant differences ($p < 0.05$) compared to CBS WT are noted by asterisk (*) or hashtag (#) in case of CBS activity in the presence of SAM.

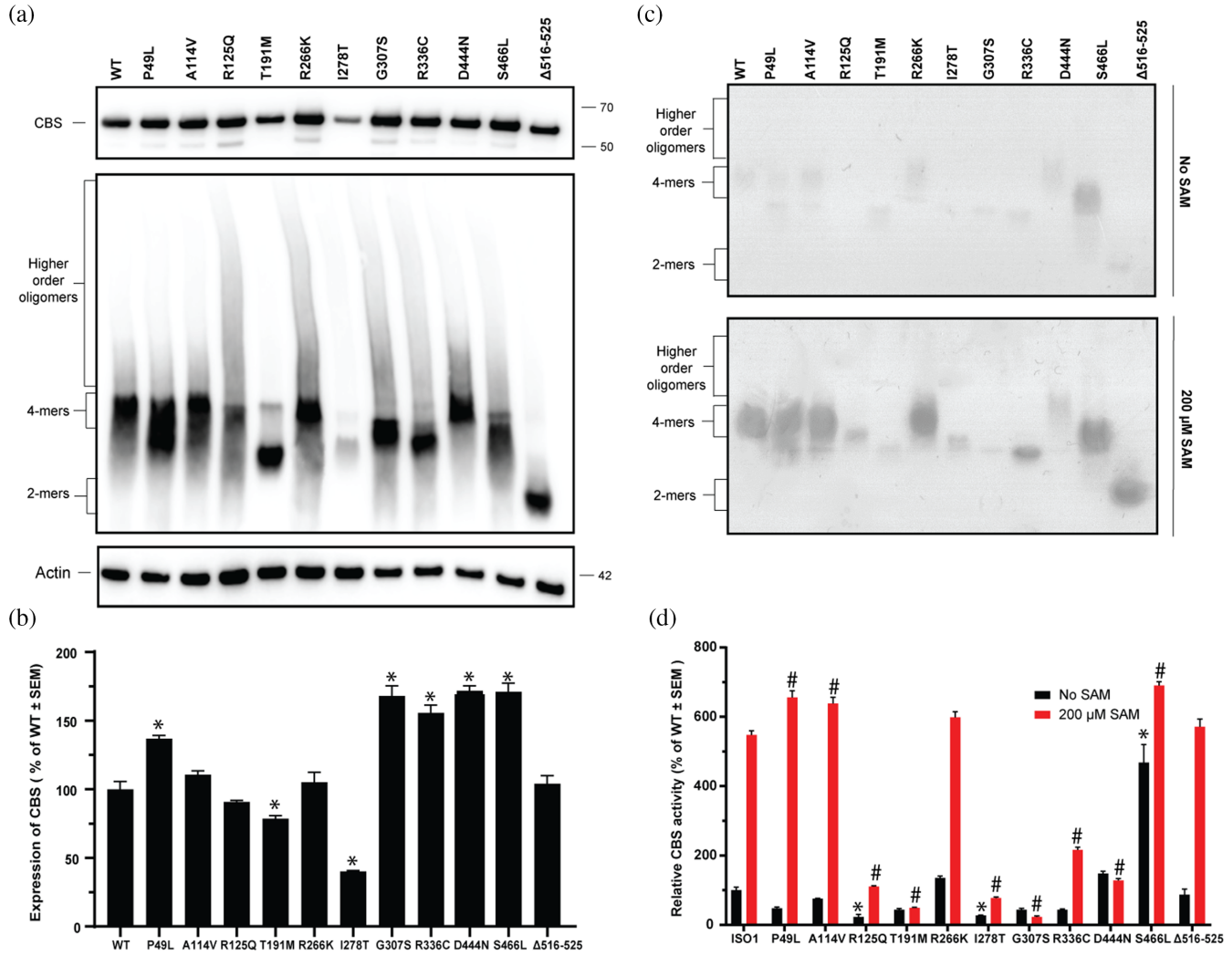

FIGURE 2 Expression of CBS variants in developed cell models of HCU. (a) Clarified lysates of HEK293A CBS KO cells stably expressing the designated CBS variant (500 ng/lane) were separated on either SDS–PAGE or native PAGE, transferred on PVDF membrane and probed for CBS or Actin. Engineered dimeric CBSΔ516-525 was used as a marker for dimeric CBS species (Ereno-Orbea et al., 2013, 2014; Pey et al., 2016). (b) Quantification of CBS expression from SDS–PAGE CBS Western blot in panel a normalized using actin. (c) In-gel CBS activity staining (10 μg/lane; c) of clarified cell lysates in the absence and presence of 200 μM SAM. (d) Quantification of active CBS oligomers from the activity staining gels shown in panel c. Significant differences ($p < 0.05$) compared to CBS WT are noted by asterisk (*) or hashtag (#) in case of CBS activity in the presence of SAM.

D444N CBS variants. In contrast, CBS T191M and G307S cell lysates showed essentially no activity (i.e., equal to background signal from equal protein amount of cell lysates from non-transformed HEK293A CBS KO cell). The CBS I278T showed the anticipated response to SAM, and CBS S466L exhibited a constitutively activated, SAM-unresponsive character (Figure 1d).

As AzMC probe senses H_2S, other cellular enzymatic sources of H_2S could potentially interfere with our CBS activity assay, namely and most importantly the second enzyme of transsulfuration pathway CGL well expressed in kidney (Kabil et al., 2011). Specifically, H_2S levels in cell lysate of HEK293 CBS KO were 19.2- and 141.5-fold lower than that in positive control expressing CBS WT when used the same protein amount in the assay (Figure S1a,b). The 20- and 30-fold higher protein input in the assay would increase level of interreference by two- and three-fold, respectively (Figure S1c). The contribution of CGL was assessed by performing the assay on cell lysates from cell overexpressing CBS WT, CBS T191M, and CBS I278T variants in the absence and presence of 3 mM PAG. Figure S1d–f shows there was clearly detectable interference of CGL at a constant level across three different cell models. However, this stable contribution was offset by normalization and relative expression of CBS activity and thus had no impact on comparison of CBS activities among different cell models presented in Figure 1. Taken together, Figure S1 shows that potential

interference from other sources of H_2S on our assay as performed was negligible.

SDS–PAGE analysis of the cell lysates followed by Western blot indicated that steady-state levels of all modeled CBS variants are similar to that of WT except the I278T variant where the protein was quantified based on SDS–PAGE being approximately 40% of CBS WT steady-state levels (Figure 2a,b). Native PAGE analysis showed that most of the HCU variants form tetramers similar to WT; however, there were several noteworthy differences as well: the T191M, I278T, R336C and to some extent P49L, A114V, G307S, and S466L CBS variants yielded faster-migrating species possibly indicating differential conformation of the tetramers or partial degradation (Figure 2a). Furthermore, all samples showed higher molecular weight "tailing"—occasionally with clearly visible discreet species—suggesting the formation of soluble higher-order oligomers.

Native conformations of CBS variants as resolved in a polyacrylamide gel were also probed for catalytic activity in the absence and presence of CBS allosteric activator SAM (Figure 2c,d). For most of the CBS variants investigated, the most prominent tetrameric band/species detected on the Western blot (Figure 2a) correlated well with the in-gel activity staining and, as expected, addition of 200 μM SAM increased the catalytic activity of the enzyme. However, T191M and G307S CBS variants showed almost no staining in both the absence and presence of SAM suggesting no or very little residual CBS activity. Furthermore, D444N and S466L CBS variants showed impaired response to SAM with CBS S466L being clearly activated already under basal conditions (Figure 2d). In general, results from the in-gel assessment of CBS activity correlated well with the results using standard in-solution assay showed in Figure 1d. In summary, we successfully generated a new cellular model of HCU by modeling 10 most common missense pathogenic mutations, which were subsequently used to characterize CBS proteostasis in HCU.

3.2 | Characterization of the cellular turnover of CBS variants

Our previous data on purified pathogenic CBS variants suggested that the kinetic stability of the C-terminal regulatory domain of the variants was significantly decreased regardless of the topology of the mutation (Pey et al., 2013). To follow up on this observation, we used our newly generated cellular models of HCU and determined the half-life of pathogenic CBS variants in their natural environment (cytoplasmic milieu) using a non-radioactive biorthogonal pulse-labeling technique. Figure 3a illustrates the employed protocol, which is an adaptation of a classical ^{35}S-labeled methionine pulse-chase experiment. Instead of a labeled methionine, the protocol exploits incorporation of L-azidohomoalanine (AHA), a biorthogonal analog of methionine, into newly synthesized proteins and metal-free "click" chemistry, where azide group of AHA specifically reacts with cyclooctyne by 1,3-dipolar cycloaddition forming stable 1,2,3-triazole conjugates. Cyclooctyne conjugated with a fluorescent dye (e.g., IRDye800-DBCO) thus specifically labels all newly synthesized proteins during AHA pulse. Protein of interest (CBS) after enrichment using immunoprecipitation is quantified over time to yield cellular half-life. It is important to note that AHA is non-toxic and its incorporation into proteins results in a highly specific labeling that does not affect ubiquitination or protein degradation (Dieterich et al., 2006). Figure 3b shows representative fluorescent gels and Western blots for WT, T191M, and I278T CBS variants used to quantify the amount of pulse-labeled CBS compared to a total CBS amount in the immunoprecipitated material normalized to CBS and actin expression in the total lysate over the 24 h chase period. The data were plotted and fitted using first-order rate kinetics, yielding rate constants of CBS stability and CBS cellular half-lives (Figure 3c). The half-life of CBS WT in our model was determined as 16.6 h. All pathogenic variants showed significantly lower half-life (i.e., diminished intracellular stability) except the N-terminal P49L and A114V CBS variants, which showed comparable half-lives as CBS WT. The least stable was CBS I278T variant with its half-life being 2.8-fold lower (5.9 h) compared to CBS WT followed by the T191M variant (2.2-fold, i.e., 7.7 h). The data indicates that cellular stability of pathogenic CBS variants is generally decreased compared to WT regardless of the topology of the missense mutation with the N-terminal mutants not being affected.

3.3 | Pathways involved in CBS degradation

Polyubiquitination of proteins serves as a general signal for their degradation, which depends on the type of polyubiquitination and is specific for a given protein (Suresh et al., 2016). Figure 4a illustrates that proteins targeted for proteasomal degradation are typically modified by covalent attachment of ubiquitin onto lysine residue and its extension forming K48-linked polyubiquitin chains. Similarly, formation of polyubiquitin chains via K6, K11, K29, and K63 usually targets the tagged protein for autophagy, ERAD, lysosomal degradation, and endocytosis/lysosomal degradation, respectively (Suresh

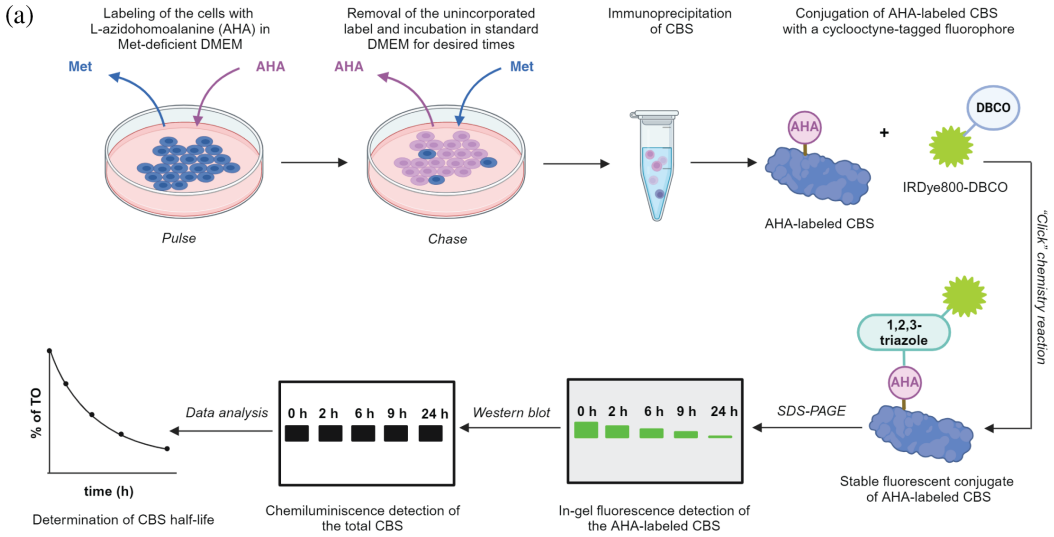

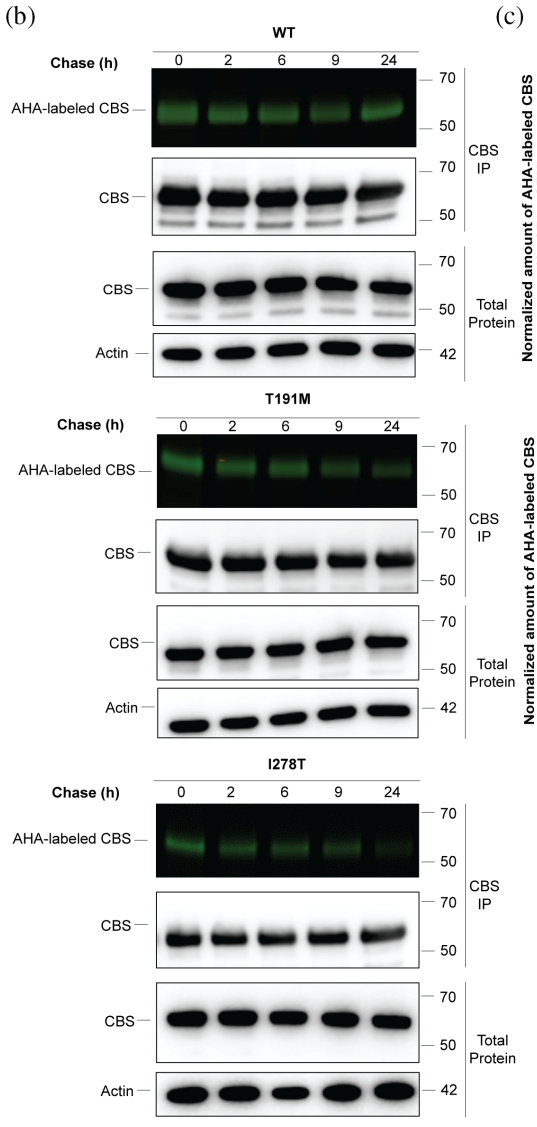

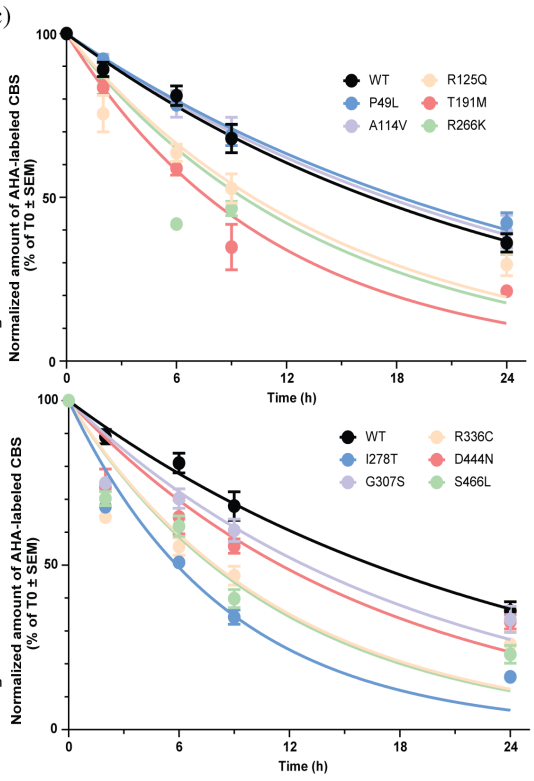

CBS variant	Rate constant (h^{-1} ± SEM)	Half-life (h ± SEM)	R^2
WT	0.042 ± 0.002	16.6 ± 0.8	0.888
P49L	0.038 ± 0.002	18.2 ± 0.9	0.956
A114V	0.040 ± 0.003	17.5 ± 1.2	0.926
R125Q	0.068 ± 0.006	10.2 ± 0.8*	0.804
T191M	0.090 ± 0.007	7.7 ± 0.6*	0.936
R266K	0.072 ± 0.009	9.6 ± 1.1*	0.776
I278T	0.118 ± 0.007	5.9 ± 0.3*	0.942
G307S	0.054 ± 0.004	12.8 ± 0.9*	0.846
R336C	0.087 ± 0.008	7.9 ± 0.7*	0.778
D444N	0.060 ± 0.005	11.5 ± 1.2*	0.742
S466L	0.089 ± 0.007	7.8 ± 0.6*	0.866

FIGURE 3 Legend on next page.

et al., 2016). Several prior studies indicated that pathogenic CBS variants are degraded via ubiquitin–proteasome system (UPS) as proteasome inhibitors rescued steady-state levels and often also activity of several pathogenic CBS variants (Gupta et al., 2013, 2019, 2023; Singh et al., 2010); however, systemic evaluation of cellular degradation pathways involved in CBS proteostasis is missing. Therefore, in the current study we systematically assessed the protein degradation pathways involved in CBS proteostasis by employing HA-tagged ubiquitin variants capable of forming polyubiquitin extensions only via the certain lysine residue(s). In addition to ubiquitin WT capable of forming polyubiquitin extensions via any of seven available lysine residues and KO unable to do any such extensions, we employed variants with mutated all lysine residues to arginines leaving just a single one available for polyubiquitination, that is, the K6, K11, K29, K48, or K63 residue (Figure 4a).

For further characterization, we selected CBS T191M and I278T variants as the most common pathogenic alleles with substantially affected cellular turnover (Figure 3), representing clinically severe pyridoxine-unresponsive and mild responsive forms of HCU, respectively. Figure 4b shows the delineation of the degradation pathways for CBS WT serving as a control establishing the proteostasis of properly folded CBS, while Figure 4c,d depicts the respective analysis for pathogenic CBS T191M and I278T variants. Accumulation of ubiquitinated CBS above the levels observed for ubiquitin WT indicates the lack of CBS degradation directed by polyubiquitination of the specific lysine residue and could result in exclusion of the specific degradation pathway. Conversely, diminished banding and/or overall signal after transient indicated increased CBS degradation signaled by polyubiquitination via the certain lysine residue, this suggesting potential pathway involved in CBS proteostasis. Following pulldown of all HA-ubiquitin-tagged proteins by immunoprecipitation and detection of CBS by Western blot, we typically observed a major band around 80 kDa likely corresponding to a monoubiquitinated CBS and additional higher bands corresponding to polyubiquitinated CBS polypeptides. Ubiquitinated CBS was substantially and significantly diminished for all three CBS variants co-expressing the K48-ubiquitin mutant compared to those co-expressing WT-ubiquitin (Figure 4b–d). This result indicates that UPS is the major pathway responsible for CBS proteostasis in health (CBS WT) and HCU (CBS T191M and I278T). However, co-expression of K11-ubiquitin showed similar recovery of CBS T191M variant as WT-ubiquitin, suggesting that the ERAD pathway could be involved in proteostasis of this pathogenic CBS variant (Figure 4c). On the other hand, co-expression of K63-ubiquitin showed significantly decreased the recovery of CBS I278T variant compared to WT-ubiquitin, suggesting that the lysosomal pathway could play a role in in proteostasis of CBS I278T variant (Figure 4d).

3.4 | Rescue of CBS stability and activity by pharmacological modulation of proteostasis

After identification of UPS as the major CBS degradation pathway and ERAD or lysosomal degradation as minor pathways involved in proteostasis of pathogenic CBS variants, we pharmacologically modulated these pathways, in order to restore the half-life and/or activity of the CBS variants. Figure 5a–c shows representative fluorescent gels and Western blots for WT, T191M, and I278T CBS variants used to quantify the amount of CBS for determination of half-life when cells were treated for up to 24 h with a proteasome inhibitor (20 nM bortezomib; BRB), an ALP inhibitor (100 nM bafilomycin; BAF) or an ERAD inhibitor (10 μM eeyarestatin I; ESI). Quantified and normalized data were subsequently plotted and fitted using first-order rate kinetics fit yielding rate constants and half-lives of CBS variants after treatment (Figure 5d–f). Consistent with prior literature (Gupta et al., 2013, 2019, 2023; Singh et al., 2010), UPS was found to play a significant role in CBS proteostasis (Figure 4): treatment with bortezomib significantly increased half-life of CBS WT by 7.7-fold as well as pathogenic CBS variants CBS T191M by 6.8-fold and CBS I278T by 3.0-fold (Figure 5d). Treatment with bafilomycin had no effect on CBS T191M variant, but it significantly increased the half-life of CBS WT and CBS I278T by 1.4-fold and 1.6-fold, respectively (Figure 5e). Treatment with eeyarestatin I had similar impact as bafilomycin: this inhibitor exerted no effect in case of CBS T191M, but increased

FIGURE 3 Cellular turnover of CBS. (a) Schematic representation of the employed pulse-chase experiment. (b) Representative images of fluorescent gels and Western blots for both CBS immunoprecipitates and total protein fractions (500 ng/lane) of CBS WT, T191M, and I278T variants at the designated timepoints (0, 2, 6, 9, and 24 h after the AHA labeling) used for quantification and normalization of the pulse-labeled CBS compared to the total CBS amounts. (c) Plots of first-order rate kinetics fit of the data from AHA pulse-chase experiments and table summarizing obtained CBS stability rate constants and CBS half-lives. Significant differences ($p < 0.05$) compared to CBS WT are noted by asterisk (*).

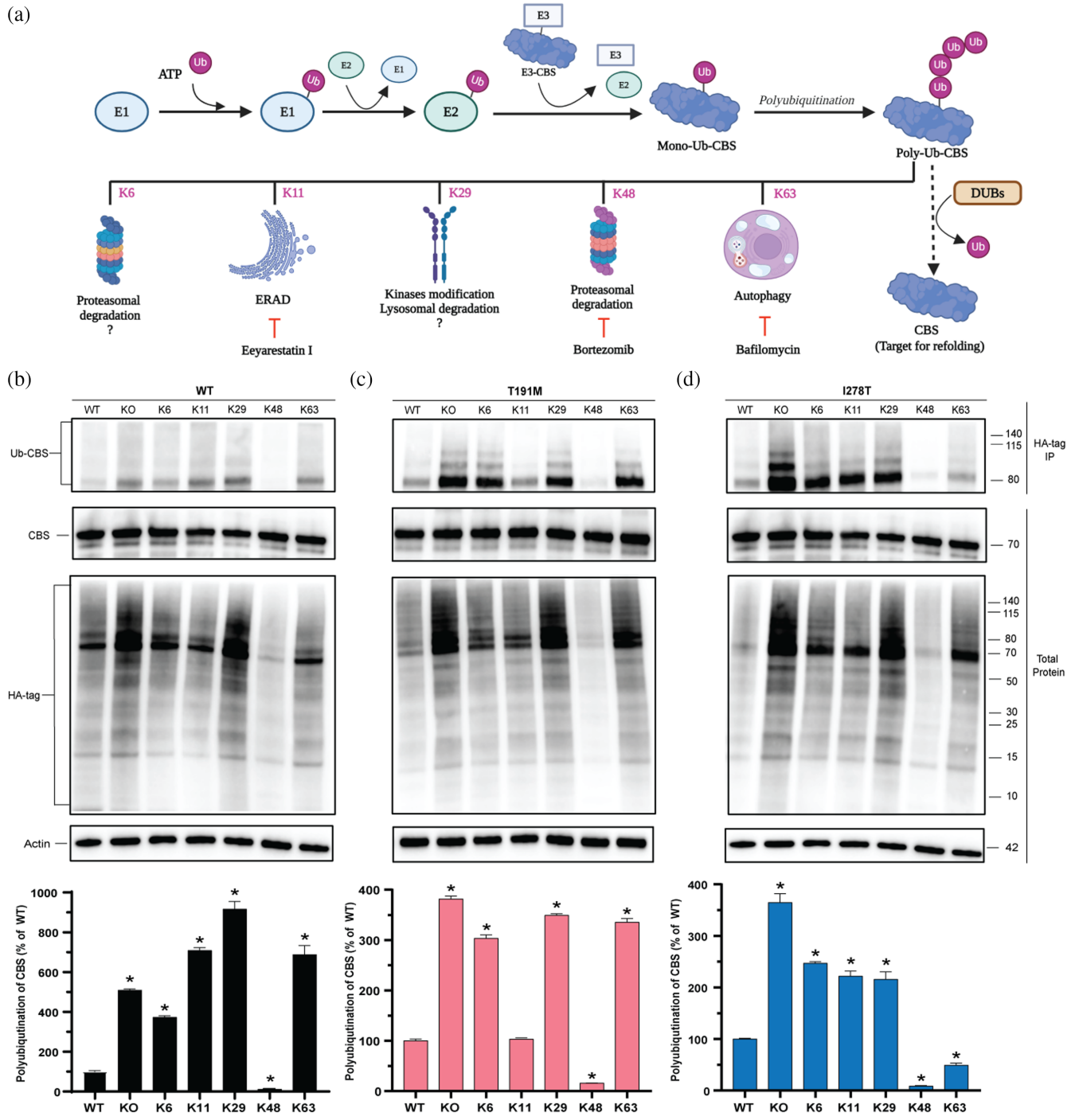

FIGURE 4 Pathways involved in degradation of CBS. (a) Schematic representation of protein function and stability regulated by the ubiquitination. While monoubiquitination typically signals endocytosis, DNA repair or trafficking, polyubiquitination via the certain lysine residue often determines the degradation pathway of the protein. (b–d) Assessment of polyubiquitination-regulated degradation pathways for CBS WT (b), T191M (c), and I278T variants (d) using co-expression with the specific HA-tagged ubiquitin variants. Representative images of Western blots for both HA-tag immunoprecipitates and total protein fractions (500 ng/lane) probed with antibodies as indicated. Quantification of ubiquitinated CBS in the immunoprecipitates shows significant differences compared to the respective CBS variant co-expressed with HA-tagged ubiquitin WT as a control (*$p < 0.05$).

the half-life of CBS WT by 1.4-fold and the half-life of CBS I278T by 1.6-fold (Figure 5f). These data suggest that UPS is the major degradation pathway for all CBS variants, while ALP and ERAD have smaller contributions, which are selective for CBS WT and I278T variant, but not for the T191M variant.

Next, we sought to determine if the increase in half-life of CBS variants correlates with a rescue of their

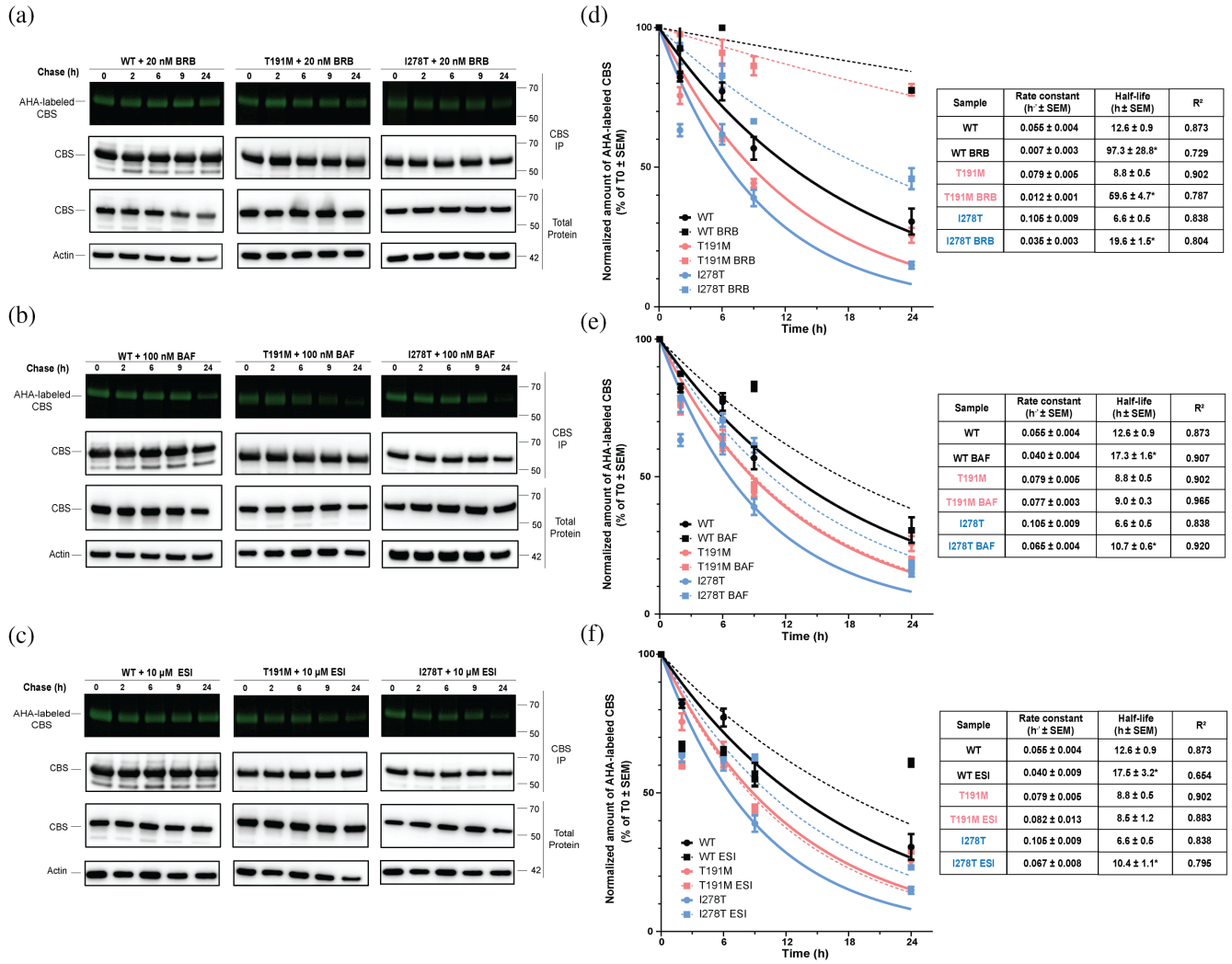

Sample	Rate constant (h^{-1} ± SEM)	Half-life (h ± SEM)	R^2
WT	0.055 ± 0.004	12.6 ± 0.9	0.873
WT BRB	0.007 ± 0.003	97.3 ± 28.8*	0.729
T191M	0.079 ± 0.005	8.8 ± 0.5	0.902
T191M BRB	0.012 ± 0.001	59.6 ± 4.7*	0.787
I278T	0.105 ± 0.009	6.6 ± 0.5	0.838
I278T BRB	0.035 ± 0.003	19.6 ± 1.6*	0.804

Sample	Rate constant (h^{-1} ± SEM)	Half-life (h ± SEM)	R^2
WT	0.055 ± 0.004	12.6 ± 0.9	0.873
WT BAF	0.040 ± 0.004	17.3 ± 1.6*	0.907
T191M	0.079 ± 0.005	8.8 ± 0.5	0.902
T191M BAF	0.077 ± 0.003	9.0 ± 0.3	0.965
I278T	0.105 ± 0.009	6.6 ± 0.5	0.838
I278T BAF	0.065 ± 0.004	10.7 ± 0.6*	0.920

Sample	Rate constant (h^{-1} ± SEM)	Half-life (h ± SEM)	R^2
WT	0.055 ± 0.004	12.6 ± 0.9	0.873
WT ESI	0.040 ± 0.009	17.5 ± 3.2*	0.654
T191M	0.079 ± 0.005	8.8 ± 0.5	0.902
T191M ESI	0.082 ± 0.013	8.5 ± 1.2	0.883
I278T	0.105 ± 0.009	6.6 ± 0.5	0.838
I278T ESI	0.067 ± 0.008	10.4 ± 1.1*	0.795

FIGURE 5 Pharmacological rescue of CBS stability. (a)–(c) Representative images of fluorescent gels and Western blots for both CBS immunoprecipitates and total protein fractions (500 ng/lane) of CBS WT, T191M, and I278T variants at the designated timepoints (0, 2, 6, 9, and 24 h after the AHA labeling) in the vehicle (DMSO)-treated cells used as controls and cells treated with 20 nM bortezomib (BRB; a), 100 nM bafilomycin (BAF; b) or 10 μM eeyarestatin I (ESI; c). The gels and blots were used for quantification and normalization of the pulse-labeled CBS compared to the total CBS amounts. (d–f) Plots of first-order rate kinetics fit of the data from AHA pulse-chase experiments of CBS WT, T191M, and I278T variants and table summarizing obtained CBS stability rate constants and CBS half-lives in the in the vehicle (DMSO)-treated cells used as controls and cells treated with 20 nM bortezomib (d), 100 nM bafilomycin (e), or 10 μM eeyarestatin I (f). Significant differences ($p < 0.05$) compared to respective vehicle-treated CBS variant are noted by asterisk (*).

enzymatic activity. To that end, we employed live cell imaging visualizing and quantifying CBS activity using H_2S-specific fluorescent probe AzMC (Figure 6). We observed a trend for increased H_2S biogenesis in CBS WT-expressing cells after 24 h treatment with 20 nM bortezomib (174%) and 10 μM eeyarestatin I (147%), but no effect of 100 nM bafilomycin (88%) compared to vehicle-treated control (Figure 6a). The cells expressing CBS T191M responded similarly to the treatments as those of CBS WT: significant increase of activity after bortezomib and eeyarestatin I treatments (259% and 244% compared to vehicle-treated CBS T191M, respectively; $p < 0.05$) with no significant impact of bafilomycin (134%; Figure 6b). All three interventions significantly rescued CBS activity of cells expressing CBS I278T variant with bortezomib, bafilomycin, and eeyarestatin I increasing H_2S-signal by 574%, 200%, and 374% compared to vehicle-treated CBS I278T, respectively ($p < 0.05$; Figure 6c). These findings correlate well with the observed effect of the treatments on cellular turnover of the studied CBS variants (Figure 5). It should be noted that the proteasome inhibitor bortezomib- and ERAD inhibitor eeyarestatin I-treated cells exhibited signs of cell damage and apoptosis indicating potential cytotoxic effect at the effective concentrations. This is consistent with prior findings in various

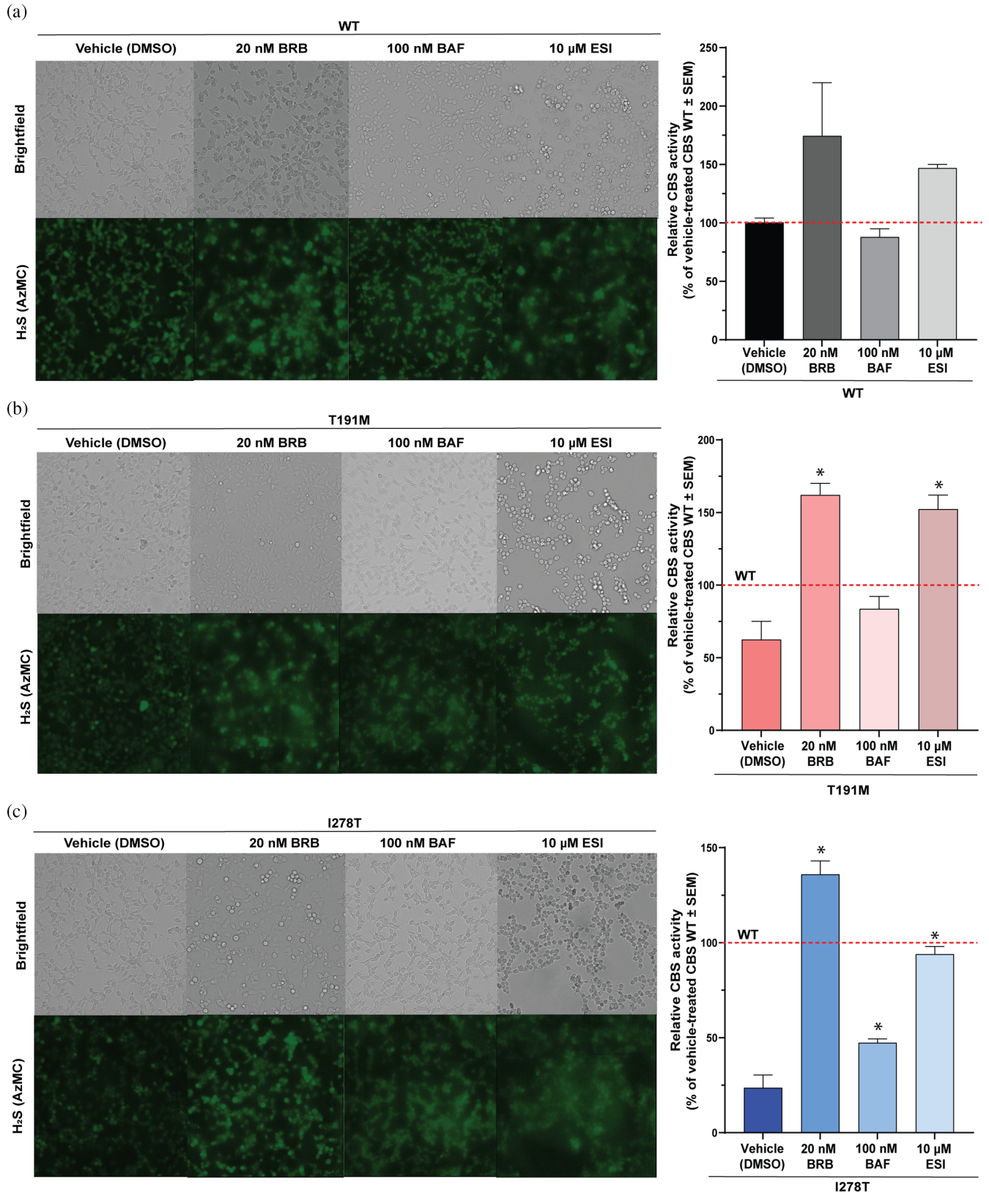

FIGURE 6 Legend on next page.

cell types (Coquelle et al., 2006; Wang et al., 2009) and it is not a surprising effect considering that these compounds induce a generalized inhibition of key protein degradation pathways.

4 | DISCUSSION

In this study, we established a new cellular model of HCU based on human HEK293 cells and utilized it to study proteostasis of CBS in health and disease. In the past, we and others have used cellular models heterologously expressing human CBS variants in bacterial cells (Kozich et al., 2010; Majtan et al., 2010), yeast (Kruger et al., 2003; Kruger & Cox, 1994; Majtan et al., 2008), mammalian Chinese hamster cells (Collard & Majtan, 2023; Maclean et al., 2002) in addition to skin fibroblasts derived from HCU patients (Janosik et al., 2001; Lipson et al., 1980; Maclean et al., 2002; Skovby et al., 1982). The bacterial models were useful for high-yield production of CBS variants for detailed biochemical and biophysical characterizations, but they are unsuitable for clarification of molecular mechanisms responsible for CBS proteostasis. The yeast model of HCU uncovered the folding environment of CBS in eukaryotic cell (Singh & Kruger, 2009), but the molecular chaperones and other effectors of protein folding and degradation machinery often differ in their presence, properties and/or functions from those in humans. Chinese hamster cells are devoid of CBS activity (Francke & Francke, 1981), thus representing a useful model for expression of human CBS variants in mammalian cells. Indeed, Chinese hamster cells heterologously expressing HCU-causing CBS variants facilitated the discovery of heme arginate acting as a pharmacological chaperone for a specific subset of CBS variants (Melenovska et al., 2015) and further improved our understanding about pharmacological rescue of CBS folding and activity as a potential treatment for HCU (Collard & Majtan, 2023). However, similar to yeast models, lack of reagents, such as primary antibodies, designed to detect non-human proteins made further analysis and interpretations challenging. Cultured skin fibroblasts from HCU patients have been studied since discovery of the disease and even used for diagnostics (genotyping, CBS enzymatic assay) (Lipson et al., 1980; Skovby et al., 1982). Interestingly, extracts from skin showed no detectable CBS activity (Uhlendorf & Mudd, 1968) suggesting that skin-derived fibroblasts express CBS only when cultured. Culturing skin fibroblasts is time-consuming, provides limited amount of sample and genetic backgrounds of each HCU and control fibroblasts differ affecting both experimentation and interpretation. Although Chinese hamster cells and skin fibroblasts were instrumental in establishing HCU as a conformational/misfolding disease, natural absence of CBS in both Chinese hamster cells and human skin fibroblasts may limit the inferences that can be drawn about the regulation and proteostasis of CBS. The HEK293 cells of human embryonic kidney origin used in the model presented in this study represent an ideal host as CBS expression is second highest in kidney after the central metabolic organ liver (Kabil et al., 2011) and have suitable growth properties (adherent monolayer, reasonably fast proliferation, well characterized, suitable for various molecular interventions). Indeed, HEK293 cells were previously used for immunohistochemical imaging studies of overexpressed human CBS variants (Casique et al., 2013) and CRISPR-Cas9 modeling of HCU (Ismail et al., 2019). Genetic knockout of intrinsic CBS and stable expression of any HCU-pathogenic CBS variant provide flexibility, robustness and utility of the present model not just for characterization of proteostasis environment of CBS, but also potential future applications, such as CBS purification or imaging.

We determined that turnover of CBS WT in our cellular model is 16.6 h using the non-radioactive biorthogonal labeling technique previously used to determine half-life of choline-O-acetyltransferase, an enzyme catalyzing synthesis of the neurotransmitter acetylcholine (Morey et al., 2016). Recent high-throughput proteomics approach determined turnover rates of over 3000 proteins in mouse tissues, including CBS in liver being around 2.5 days or 60 h (Rolfs et al., 2021). This large discrepancy is likely caused by a different model or expression levels and regulation between mouse liver and cultured human cells stably overexpressing CBS. Importantly, our assay found significantly decreased half-lives for most of the studied pathogenic CBS variants compared to CBS WT

FIGURE 6 Pharmacological rescue of CBS activity. (a–c) Representative images from live cell imaging visualizing the cells (brightfield) and CBS activity using H_2S-specific fluorescent probe AzMC (fluorescent images). The HEK293 CBS KO cells expressing CBS WT (a), T191M (b), or I278T (c) were treated with a vehicle (DMSO) or the designated proteostasis modulator (20 nM bortezomib (BRB), 100 nM bafilomycin (BAF), or 10 μM eeyarestatin I (ESI)) for 24 h, incubated with 100 μM AzMC in HBSS for 1 h and immediately visualized. Plots show quantification of AzMC signal (four different areas in the wells of three replicates) of the respective fluorescent images. Red dashed line denotes relative CBS activity of vehicle-treated CBS WT threshold. Significant differences ($p < 0.05$) compared to respective vehicle-treated CBS variant are noted by asterisk (*).

(Figure 3). This result confirms our previous observation from calorimetric characterization of the purified CBS variants that the C-terminal domains of seven studied HCU-causing CBS variants have significantly decreased kinetic stability compared to that of WT regardless of topology of the pathogenic missense mutation (Pey et al., 2013). The study thus suggested that HCU CBS variants could be less stable, which, in turn, could affect their steady-state levels and rate of degradation in cells as shown here. The two herein studied representatives of severe pyridoxine-unresponsive HCU (CBS T191M) and typically mild pyridoxine-responsive HCU (CBS I278T) were not previously characterized using calorimetric approach or other biochemical assays due to the inability to purify these CBS variants to homogeneity in sufficient quantities. They showed the highest cellular turnover from the set of CBS variants (Figure 3c) and together with a kinetically stable, but catalytically incompetent CBS G307S the lowest catalytic activity (Figures 1d and 2c,d), which in summary suggest the reasons for being not amenable for purification and their detailed biochemical and biophysical characterization.

Rapid degradation of dysfunctional, misfolded CBS has been observed previously in both cellular and animal models of HCU (Gupta et al., 2013, 2019; Melenovska et al., 2015; Singh & Kruger, 2009). However, there seems to be no statistically significant correlation between the percentage of residual CBS activity of pathogenic CBS variants compared to WT and the amount of CBS protein (Skovby et al., 1982). These data suggest that the mutation and its specific impact on CBS protein can uniquely impair proteostasis of CBS. Indeed, a previous study on HCU fibroblasts showed that pathogenic CBS variants are prone to form soluble high-molecular weight aggregates rather than native tetramers compared to CBS WT (Janosik et al., 2001). Different oligomeric tendencies of active CBS WT and catalytically impaired misfolded HCU CBS variants would be expected to affect CBS proteostasis, in particular degradation pathways. Our data demonstrate that CBS WT is essentially solely degraded via UPS, while the degradation of pathogenic CBS variants also involves ERAD or ALP (Figure 4). Utilization of these two alternative pathways to dispose of pathogenic CBS variants may potentially be related to the induction of ER stress due to CBS misfolding and aggregation (or formation of higher-molecular weight complexes). Previously we showed that the expression of CBS I278T variant significantly upregulates expression of several cytoplasmic molecular chaperones and substantially increases the expression of BiP, an ER sensor of unfolded protein response (Collard & Majtan, 2023; Cyr & Hebert, 2009) indicating involvement of ER in proteostasis of HCU CBS variants. ALP is the second main pathway for protein degradation after UPS, typically used for protein aggregates and organelles (Siva Sankar & Dengjel, 2020).

Could pharmacological manipulation of CBS proteostasis rescue folding, stability and ultimately activity of pathogenic mutants? Our data show that inhibition of proteasomal or ER-associated degradation, but not lysosomal-mediated degradation, indeed rescues the activity of CBS T191M and I278T variants (Figure 6). Interestingly, the rescue of CBS activity correlates well with a decreased turnover of the proteins in case of proteasomal inhibition, but not for ERAD suggesting that increased stability and/or cellular steady-state levels of CBS are not pre-requisite for activity rescue. Indeed, proteasome inhibitors, such as clinically used bortezomib for treatment of multiple myeloma and lymphoma, partially rescued protein expression and activity of several pathogenic CBS variants modeled in transgenic mice including I278T and T191M (Gupta et al., 2013, 2023). It is important to note that these transgenic HCU mice showed a fairly heterogenous response to acute treatment with bortezomib—with some mice responding to treatment by increased protein levels and activity as well as decreased plasma total homocysteine concentration, while other mice did not respond at all. Although the root cause of this heterogeneity is unclear at present, it is worth emphasizing that there was a close correlation with the levels of properly folded CBS, that is, the amounts of native CBS tetramers rather than total CBS amounts (Gupta et al., 2013). In addition, lower doses of proteasome inhibitors provided over the extended period of time compared to acute dosing with the pharmacologically effective dose showed significantly lower efficacy in decreasing plasma total homocysteine. Therefore, reducing toxicity of proteasome inhibitors for chronic administration by lowering their dose seem ineffective as a monotherapy for HCU. Whether a combination of low-dose proteasome inhibitors with other general modulators of proteostasis, such as activators of molecular chaperones, or more specific CBS pharmacological chaperones including pyridoxine could result in significant rescue of CBS activity and correction of metabolic imbalance in HCU, that remains to be tested in future experiments.

Taken together, our results provide new insights into CBS proteostasis under physiological and pathological HCU conditions. As adoption of native-like CBS conformation and its assembly into active oligomers (rather than total amount of CBS) correlated better with rescue of CBS activity, future work should focus on correction of folding of pathogenic CBS variants in search of specific pharmacological chaperones or combination of pharmacological interventions in order to discover novel ways how to address unmet need of HCU.

AUTHOR CONTRIBUTIONS

Ela Mijatovic: Investigation; formal analysis; visualization; writing – original draft; writing – review and editing; validation; data curation. **Kelly Ascenção:** Methodology; investigation; writing – review and editing. **Csaba Szabo:** Resources; writing – review and editing; supervision; funding acquisition. **Tomas Majtan:** Conceptualization; methodology; visualization; supervision; project administration; resources; writing – original draft; writing – review and editing; funding acquisition.

ACKNOWLEDGMENTS

T. M. acknowledges support from the University of Fribourg (Research Pool grant 22-15) and the Swiss National Science Foundation (project funding 10.001.133).

CONFLICT OF INTEREST STATEMENT

The authors declare no conflicts of interest.

ORCID

Tomas Majtan https://orcid.org/0000-0002-2751-2124

REFERENCES

Araki K, Nagata K. Protein folding and quality control in the ER. Cold Spring Harb Perspect Biol. 2011;3:a007526.

Ascencao K, Dilek N, Augsburger F, Panagaki T, Zuhra K, Szabo C. Pharmacological induction of mesenchymal–epithelial transition via inhibition of H_2S biosynthesis and consequent suppression of ACLY activity in colon cancer cells. Pharmacol Res. 2021;165:105393.

Asimakopoulou A, Panopoulos P, Chasapis CT, Coletta C, Zhou Z, Cirino G, et al. Selectivity of commonly used pharmacological inhibitors for cystathionine beta synthase (CBS) and cystathionine gamma lyase (CSE). Br J Pharmacol. 2013;169:922–32.

Balchin D, Hayer-Hartl M, Hartl FU. Recent advances in understanding catalysis of protein folding by molecular chaperones. FEBS Lett. 2020;594:2770–81.

Casili G, Randi E, Panagaki T, Zuhra K, Petrosino M, Szabo C. Inhibition of the 3-mercaptopyruvate sulfurtransferase-hydrogen sulfide system promotes cellular lipid accumulation. Geroscience. 2022;44:2271–89.

Casique L, Kabil O, Banerjee R, Martinez JC, De Lucca M. Characterization of two pathogenic mutations in cystathionine beta-synthase: different intracellular locations for wild-type and mutant proteins. Gene. 2013;531:117–24.

Chen J, Garssen J, Redegeld F. The efficacy of bortezomib in human multiple myeloma cells is enhanced by combination with omega-3 fatty acids DHA and EPA: timing is essential. Clin Nutr. 2021;40:1942–53.

Cirino G, Szabo C, Papapetropoulos A. Physiological roles of hydrogen sulfide in mammalian cells, tissues, and organs. Physiol Rev. 2023;103:31–276.

Collard R, Majtan T. Genetic and pharmacological modulation of cellular proteostasis leads to partial functional rescue of homocystinuria-causing cystathionine-beta synthase variants. Mol Cell Biol. 2023;43:664–74.

Coquelle A, Mouhamad S, Pequignot MO, Braun T, Carvalho G, Vivet S, et al. Cell cycle-dependent cytotoxic and cytostatic effects of bortezomib on colon carcinoma cells. Cell Death Differ. 2006;13:873–5.

Cyr DM, Hebert DN. Protein quality control—linking the unfolded protein response to disease. Conference on 'From unfolded proteins in the endoplasmic reticulum to disease'. EMBO Rep. 2009;10:1206–10.

Dieterich DC, Link AJ, Graumann J, Tirrell DA, Schuman EM. Selective identification of newly synthesized proteins in mammalian cells using bioorthogonal noncanonical amino acid tagging (BONCAT). Proc Natl Acad Sci U S A. 2006;103:9482–7.

Ereno-Orbea J, Majtan T, Oyenarte I, Kraus JP, Martinez-Cruz LA. Structural basis of regulation and oligomerization of human cystathionine beta-synthase, the central enzyme of transsulfuration. Proc Natl Acad Sci U S A. 2013;110:E3790–9.

Ereno-Orbea J, Majtan T, Oyenarte I, Kraus JP, Martinez-Cruz LA. Structural insight into the molecular mechanism of allosteric activation of human cystathionine beta-synthase by S-adenosylmethionine. Proc Natl Acad Sci U S A. 2014;111:E3845–52.

Francke U, Francke B. Requirement of the human chromosome 11 long arm for replication of herpes simplex virus type 1 in nonpermissive Chinese hamster × human diploid fibroblast hybrids. Somatic Cell Genet. 1981;7:171–91.

Gelman JS, Sironi J, Berezniuk I, Dasgupta S, Castro LM, Gozzo FC, et al. Alterations of the intracellular peptidome in response to the proteasome inhibitor bortezomib. PLoS One. 2013;8:e53263.

Gupta S, Wang L, Anderl J, Slifker MJ, Kirk C, Kruger WD. Correction of cystathionine beta-synthase deficiency in mice by treatment with proteasome inhibitors. Hum Mutat. 2013;34:1085–93.

Gupta S, Wang L, Kruger WD. The c.797 G>A (p.R266K) cystathionine beta-synthase mutation causes homocystinuria by affecting protein stability. Hum Mutat. 2017;38:863–9.

Gupta S, Gallego-Villar L, Wang L, Lee HO, Nasrallah G, Al-Dewik N, et al. Analysis of the Qatari R336C cystathionine beta-synthase protein in mice. J Inherit Metab Dis. 2019;42:831–8.

Gupta S, Lee HO, Wang L, Kruger WD. Examination of two different proteasome inhibitors in reactivating mutant human cystathionine beta-synthase in mice. PLoS One. 2023;18:e0286550.

Hnizda A, Majtan T, Liu L, Pey AL, Carpenter JF, Kodicek M, et al. Conformational properties of nine purified cystathionine beta-synthase mutants. Biochemistry-US. 2012;51:4755–63.

Ismail HM, Krishnamoorthy N, Al-Dewik N, Zayed H, Mohamed NA, Giacomo VD, et al. In silico and in vivo models for Qatari-specific classical homocystinuria as basis for development of novel therapies. Hum Mutat. 2019;40:230–40.

Janosik M, Oliveriusova J, Janosikova B, Sokolova J, Kraus E, Kraus JP, et al. Impaired heme binding and aggregation of mutant cystathionine beta-synthase subunits in homocystinuria. Am J Hum Genet. 2001;68:1506–13.

Jayaraj GG, Hipp MS, Hartl FU. Functional modules of the proteostasis network. Cold Spring Harb Perspect Biol. 2020;12:a033951.

Kabil O, Vitvitsky V, Xie P, Banerjee R. The quantitative significance of the transsulfuration enzymes for H2S production in murine tissues. Antioxid Redox Signal. 2011;15:363–72.

Kaur B, Sharma PK, Chatterjee B, Bissa B, Nattarayan V, Ramasamy S, et al. Defective quality control autophagy in hyperhomocysteinemia promotes ER stress and consequent neuronal apoptosis through proteotoxicity. Cell Commun Signal. 2023;21:258.

Kozich V, Sokolova J, Klatovska V, Krijt J, Janosik M, Jelinek K, et al. Cystathionine beta-synthase mutations: effect of mutation topology on folding and activity. Hum Mutat. 2010;31:809–19.

Kraus JP, Rosenberg LE. Cystathionine beta-synthase from human liver: improved purification scheme and additional characterization of the enzyme in crude and pure form. Arch Biochem Biophys. 1983;222:44–52.

Kruger WD, Cox DR. A yeast system for expression of human cystathionine b-synthase: structural and functional conservation of the human and yeast genes. Proc Natl Acad Sci USA. 1994;91:6614–8.

Kruger WD, Wang L, Jhee KH, Singh RH, Elsas LJ 2nd. Cystathionine beta-synthase deficiency in Georgia (USA): correlation of clinical and biochemical phenotype with genotype. Hum Mutat. 2003;22:434–41.

Lim KL, Chew KC, Tan JM, Wang C, Chung KK, Zhang Y, et al. Parkin mediates nonclassical, proteasomal-independent ubiquitination of synphilin-1: implications for Lewy body formation. J Neurosci. 2005;25:2002–9.

Lipson MH, Kraus J, Rosenberg LE. Affinity of cystathionine b-synthase for pyridoxal 5′-phosphate in cultured cells. A mechanism for pyridoxine-responsive homocystinuria. J Clin Investig. 1980;66:188–93.

Livingston CM, Ifrim MF, Cowan AE, Weller SK. Virus-induced chaperone-enriched (VICE) domains function as nuclear protein quality control centers during HSV-1 infection. PLoS Pathog. 2009;5:e1000619.

Maclean KN, Gaustadnes M, Oliveriusova J, Janosik M, Kraus E, Kozich V, et al. High homocysteine and thrombosis without connective tissue disorders are associated with a novel class of cystathionine beta-synthase (CBS) mutations. Hum Mutat. 2002;19:641–55.

Majtan T, Singh LR, Wang L, Kruger WD, Kraus JP. Active cystathionine beta-synthase can be expressed in heme-free systems in the presence of metal-substituted porphyrins or a chemical chaperone. J Biol Chem. 2008;283:34588–95.

Majtan T, Liu L, Carpenter JF, Kraus JP. Rescue of cystathionine beta-synthase (CBS) mutants with chemical chaperones: purification and characterization of eight CBS mutant enzymes. J Biol Chem. 2010;285:15866–73.

Majtan T, Krijt J, Sokolova J, Krizkova M, Ralat MA, Kent J, et al. Biogenesis of hydrogen sulfide and thioethers by cystathionine beta-synthase. Antioxid Redox Signal. 2018;28:311–23.

McCorvie TJ, Adamoski D, Machado RAC, Tang J, Bailey HJ, Ferreira DSM, et al. Architecture and regulation of filamentous human cystathionine beta-synthase. Nat Commun. 2024;15:2931.

McKibbin C, Mares A, Piacenti M, Williams H, Roboti P, Puumalainen M, et al. Inhibition of protein translocation at the endoplasmic reticulum promotes activation of the unfolded protein response. Biochem J. 2012;442:639–48.

Melenovska P, Kopecka J, Krijt J, Hnizda A, Rakova K, Janosik M, et al. Chaperone therapy for homocystinuria: the rescue of CBS mutations by heme arginate. J Inherit Metab Dis. 2015;38:287–94.

Morey TM, Albers S, Shilton BH, Rylett RJ. Enhanced ubiquitination and proteasomal degradation of catalytically deficient human choline acetyltransferase mutants. J Neurochem. 2016;137:630–46.

Morey TM, Esmaeili MA, Duennwald ML, Rylett RJ. SPAAC pulse-chase: a novel click chemistry-based method to determine the half-life of cellular proteins. Front Cell Dev Biol. 2021;9:722560.

Morris AA, Kozich V, Santra S, Andria G, Ben-Omran TI, Chakrapani AB, et al. Guidelines for the diagnosis and management of cystathionine beta-synthase deficiency. J Inherit Metab Dis. 2017;40:49–74.

Mudd SH, Skovby F, Levy HL, Pettigrew KD, Wilcken B, Pyeritz RE, et al. The natural history of homocystinuria due to cystathionine b-synthase deficiency. Am J Hum Genet. 1985;37:1–31.

Panagaki T, Randi EB, Augsburger F, Szabo C. Overproduction of H2S, generated by CBS, inhibits mitochondrial complex IV and suppresses oxidative phosphorylation in Down syndrome. Proc Natl Acad Sci U S A. 2019;116:18769–71.

Panagaki T, Lozano-Montes L, Janickova L, Zuhra K, Szabo MP, Majtan T, et al. Overproduction of hydrogen sulfide, generated by cystathionine beta-synthase, disrupts brain wave patterns and contributes to neurobehavioral dysfunction in a rat model of down syndrome. Redox Biol. 2022;51:102233.

Park HJ, Ryu D, Parmar M, Giasson BI, McFarland NR. The ER retention protein RER1 promotes alpha-synuclein degradation via the proteasome. PLoS One. 2017;12:e0184262.

Petrosino M, Zuhra K, Kopec J, Hutchin A, Szabo C, Majtan T. H2S biogenesis by cystathionine beta-synthase: mechanism of inhibition by aminooxyacetic acid and unexpected role of serine. Cell Mol Life Sci. 2022;79:438.

Pey AL, Majtan T, Sanchez-Ruiz JM, Kraus JP. Human cystathionine beta-synthase (CBS) contains two classes of binding sites for S-adenosylmethionine (SAM): complex regulation of CBS activity and stability by SAM. Biochem J. 2013;449:109–21.

Pey AL, Martinez-Cruz LA, Kraus JP, Majtan T. Oligomeric status of human cystathionine beta-synthase modulates AdoMet binding. FEBS Lett. 2016;590:4461–71.

Purnell PR, Fox HS. Autophagy-mediated turnover of dynamin-related protein 1. BMC Neurosci. 2013;14:86.

Rolfs Z, Frey BL, Shi X, Kawai Y, Smith LM, Welham NV. An atlas of protein turnover rates in mouse tissues. Nat Commun. 2021;12:6778.

Sen S, Kawahara B, Mahata SK, Tsai R, Yoon A, Hwang L, et al. Cystathionine: a novel oncometabolite in human breast cancer. Arch Biochem Biophys. 2016;604:95–102.

Singh LR, Kruger WD. Functional rescue of mutant human cystathionine beta-synthase by manipulation of Hsp26 and Hsp70 levels in *Saccharomyces cerevisiae*. J Biol Chem. 2009;284:4238–45.

Singh LR, Gupta S, Honig NH, Kraus JP, Kruger WD. Activation of mutant enzyme function in vivo by proteasome inhibitors and treatments that induce Hsp70. PLoS Genet. 2010;6:e1000807.

Singh S, Padovani D, Leslie RA, Chiku T, Banerjee R. Relative contributions of cystathionine beta-synthase and gamma-

cystathionase to H_2S biogenesis via alternative trans-sulfuration reactions. J Biol Chem. 2009;284:22457–66.

Siva Sankar D, Dengjel J. Protein complexes and neighborhoods driving autophagy. Autophagy. 2020;1:2689–705.

Skovby F, Kraus J, Redlich C, Rosenberg LE. Immunochemical studies on cultured fibroblasts from patients with homocystinuria due to cystathionine b-synthase deficiency. Am J Hum Genet. 1982;34:73–83.

Suresh B, Lee J, Kim H, Ramakrishna S. Regulation of pluripotency and differentiation by deubiquitinating enzymes. Cell Death Differ. 2016;23:1257–64.

Szabo C, Coletta C, Chao C, Modis K, Szczesny B, Papapetropoulos A, et al. Tumor-derived hydrogen sulfide, produced by cystathionine-beta-synthase, stimulates bioenergetics, cell proliferation, and angiogenesis in colon cancer. Proc Natl Acad Sci U S A. 2013;110:12474–9.

Thorson MK, Majtan T, Kraus JP, Barrios AM. Identification of cystathionine beta-synthase inhibitors using a hydrogen sulfide selective probe. Angew Chem Int Ed Engl. 2013;52:4641–4.

Uhlendorf BW, Mudd SH. Cystathionine synthase in tissue culture derived from human skin: enzyme defect in homocystinuria. Science. 1968;160:1007–9.

Wang Q, Mora-Jensen H, Weniger MA, Perez-Galan P, Wolford C, Hai T, et al. ERAD inhibitors integrate ER stress with an epigenetic mechanism to activate BH3-only protein NOXA in cancer cells. Proc Natl Acad Sci U S A. 2009;106:2200–5.

Willhardt I, Wiederanders B. Activity staining of cystathionine-beta-synthetase and related enzymes. Anal Biochem. 1975;63:263–6.

Yamamoto A, Tagawa Y, Yoshimori T, Moriyama Y, Masaki R, Tashiro Y. Bafilomycin A1 prevents maturation of autophagic vacuoles by inhibiting fusion between autophagosomes and lysosomes in rat hepatoma cell line, H-4-II-E cells. Cell Struct Funct. 1998;23:33–42.

Zuhra K, Augsburger F, Majtan T, Szabo C. Cystathionine-beta-synthase: molecular regulation and pharmacological inhibition. Biomolecules. 2020;10:697.

SUPPORTING INFORMATION

Additional supporting information can be found online in the Supporting Information section at the end of this article.

How to cite this article: Mijatovic E, Ascenção K, Szabo C, Majtan T. Cellular turnover and degradation of the most common missense cystathionine beta-synthase variants causing homocystinuria. Protein Science. 2024;33(8):e5123. https://doi.org/10.1002/pro.5123

FIGURE S1. H_2S-producing activity of new cellular models of HCU. (a) Raw AzMC fluorescence readout from the CBS activity assay in HEK293A WT (original cell line with intact intrinsic CBS), HEK293A CBS KO (cell line with genetically knocked out intrinsic CBS used for generation of new cell models of HCU) and HEK293A CBSKO + CBS WT (control cell line overexpressing CBS WT on a background of no intrinsic CBS in HEK293A) as specified in Section 2. For all samples, 10 μg of cell lysate was used for each assay performed in three biological and three technical replicates. (b) Calculated slopes from raw AzMC fluorescence readouts shown in panel a. (c) Impact of protein input on CBS activity assay. Cell lysates (up to 300 μg per assay) of HEK293A WT and HEK293A CBS KO cells were analyzed using AzMC activity assay in the absence and presence of 200 μM SAM in three biological and three technical replicates. Calculated slopes from the raw fluorescence readouts over 90 min assay were compared. (d) Raw AzMC fluorescence readout from the CBS activity assay in HEK293A CBS KO cells overexpressing CBS WT, CBS T191M or CBS I278T variant in the absence or presence of 200 μM SAM. Potential contribution of cystathionine gamma-lyase was assessed by running the assay in the absence and presence of 3 mM propargylglycine (PAG), a specific CGL inhibitor. For all samples, 10 μg of cell lysate was used for each assay performed in three biological and three technical replicates. (e) Calculated slopes from raw AzMC fluorescence readouts shown in panel D. (f) Contribution of CGL on AzMC CBS activity assay expressed as difference (delta) in slope from the assays run in the absence versus presence of 3 mM PAG as shown in panel e.

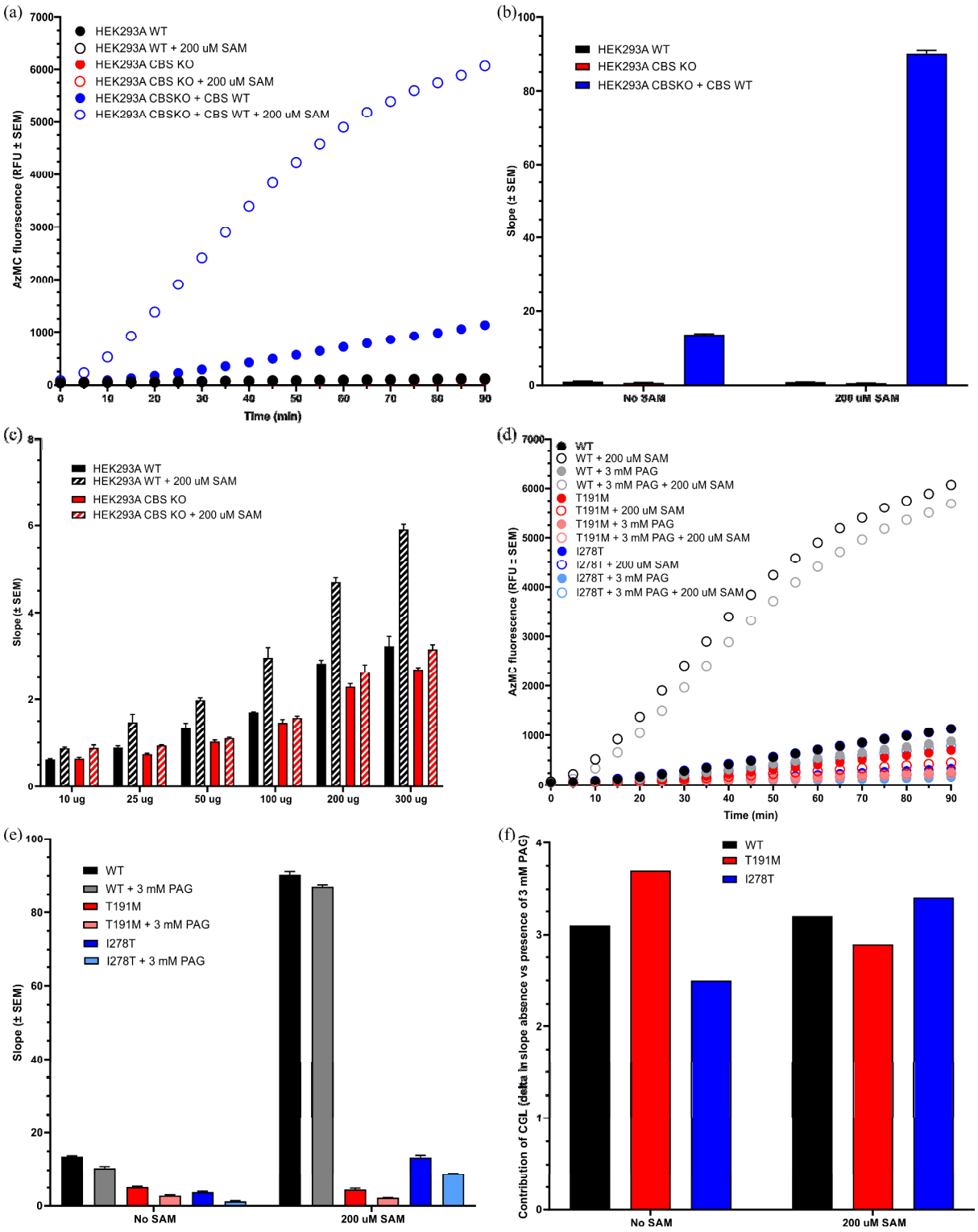
(a)
HEK293A WT
HEK293A WT + 200 uM SAM
HEK293A CBS KO
HEK293A CBS KO + 200 uM SAM
HEK293A CBSKO + CBS WT
HEK293A CBSKO + CBS WT + 200 uM SAM
AzMC fluorescence (RFU ± SEM)
Time (min)
(b)
HEK293A WT
HEK293A CBS KO
HEK293A CBSKO + CBS WT
Slope (± SEM)
No SAM
200 uM SAM
(c)
HEK293A WT
HEK293A WT + 200 uM SAM
HEK293A CBS KO
HEK293A CBS KO + 200 uM SAM
Slope (± SEM)
10 ug
25 ug
50 ug
100 ug
200 ug
300 ug
(d)
WT
WT + 200 uM SAM
WT + 3 mM PAG
WT + 3 mM PAG + 200 uM SAM
T191M
T191M + 200 uM SAM
T191M + 3 mM PAG
T191M + 3 mM PAG + 200 uM SAM
I278T
I278T + 200 uM SAM
I278T + 3 mM PAG
I278T + 3 mM PAG + 200 uM SAM
AzMC fluorescence (RFU ± SEM)
Time (min)
(e)
WT
WT + 3 mM PAG
T191M
T191M + 3 mM PAG
I278T
I278T + 3 mM PAG
Slope (± SEM)
No SAM
200 uM SAM
(f)
WT
T191M
I278T
Contribution of CGL (delta ln slope absence vs presence of 3 mM PAG)
No SAM
200 uM SAM